# Reducing velocity model uncertainty and improving microseismic event location accuracy: crosswell seismic tomography using a repeatable downhole sparker source.

*William Wills, Roger Marriage*, Avalon Sciences Ltd, James Verdon, Outer Limits Geophysics LLP.*

**Summary**

Velocity model errors are a major source of uncertainty in microseismic event location – a source of uncertainty that often goes unaddressed. This paper demonstrates how a commercial downhole sparker source can be used to produce crosswell tomography surveys that result in much improved velocity profiles. The combination of improved velocity model and more accurate event time picking deliver a much more constrained error distribution of micro seismic event location. This paper will outline a description of a repeatable and broadband downhole source, and the expected improvement to event location accuracy which is likely to be achieved, along with suggestions on how this may be applied to future monitoring surveys.

**Introduction**

Errors in microseismic event location are produced primarily by uncertainties in arrival time picks and in the velocity model (Eisner et al. 2009; Usher et al. 2013). Picking errors can easily quantified and incorporated into location uncertainties (Eisner et al. 2012). However, because the "true" velocity model cannot be simply measured (e.g. Usher et al. 2013), the uncertainties produced by an inaccurate velocity model are harder to quantify, and are therefore often dismissed.

It is common practice in earthquake seismology to invert observed event arrival times for both location and velocity model in a joint fashion (e.g. Crosson 1976). However, when monitoring microseismicity using downhole geophones it is more common to generate a fixed velocity model using well logs, perhaps calibrated using perforation shots (which have known location) where available.

The use of sonic logs to generate velocity models for microseismic event location presents a number of potential pitfalls. Sonic log measurements may be hampered by near-borehole effects, and dispersion (sonic log frequencies are typically an order of magnitude higher than seismic wavelengths). Moreover, sonic logs typically measure velocity vertically through the rock, whereas the seismic waves from microseismic events typically travel horizontally. In highly anisotropic rocks, such as shale, this may result in significant velocity model errors.

Perforation shots may be used to calibrate the sonic log-derived velocity model. However, perf-shot data provides limited information for calibration, characterizing as it does the single raypaths between shot point and the geophone array.

In contrast, a moveable, repeatable source provides much greater utility in generating and calibrating a velocity model. The source frequencies are similar to that produced by microseismic events, mitigating the effects of seismic dispersion. Waves travel sub-horizontally through the rocks of interest, mitigating the effects of anisotropy. Because both the source and the geophones can be moved easily – the geophones in both vertical and horizontal wells – waves can be shot through a greater portion of the subsurface, providing better information about the full area of interest, as opposed to a single ray-path between perf-shot and geophone array.

**Cross well surveys using a down-hole sparker source**

Cross well imaging can be achieved from a variety of downhole sources. Like all sources a consistent output acoustic signature is crucial to facilitate accurate stacked time picking and thus accurate velocity model calibration.

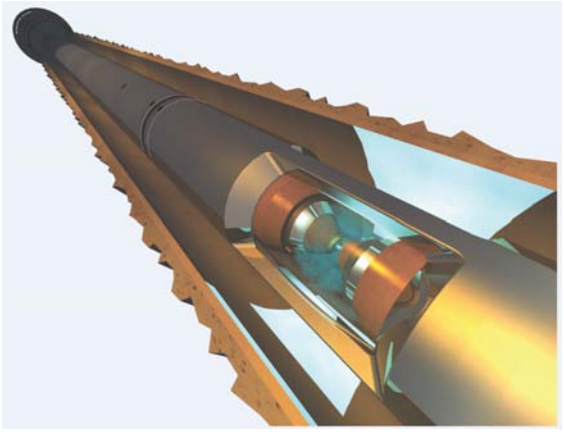

Figure 1: 3D realisation of AST electrode firing head discarging high voltage charge within borehole.

Downhole sparker tools are developed to provide a peak high energy shot (~1000+ joules) giving a repeatable high bandwidth signature. To operate a sparker tool such as the Advanced Sparker Tool (ASR) direct current power is supplied from surface to a downhole high voltage power supply unit. This in turn charges a bank of capacitors to a high voltage. When the critical voltage has been reached the energy is switched to the electrode via a gas discharge switch, generating a spark across the cathode/anode (Figure 1) and creating a high energy output pulse. The acoustic

signature is the result of the expanding and subsequent collapsing very high temperature plasma bubble oscillating through the well fluid medium providing a pressure front into the well casing in all directions (Baltazar-Lopez et al., 2009).

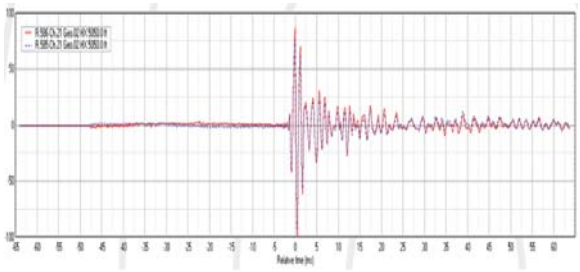

Figure 2: Unstacked time domain overlay of two consecutive AST signature shots recorded on a horizontal borehole geophone component in the D1-D2 Well, North Belt Texas (20m lateral offset).

Once depleted of charge the power supply unit proceeded to charge the capacitors downhole and the source can be re-fired. This process takes ~15-20s with the 5000v pulse providing a consistent output signature (Figure 2).

**Survey Configuration**

In this paper we seek to compare velocity models produced from well log data and from a sparker source cross-well survey acquired from the cased D1 and D2 wells of the wells of Halliburton's North Belt Test facility, Texas, USA. The ASR sparker source was deployed within the vertical D1 well to a depth of 1510m MD. The borehole seismic string, a 3 component borehole receiver System (Avalon Geochain) was locked in to position at 1400m within the cased gently deviated D2 well. The recording system comprised of 8 receiver satellites with 15m vertical spacing. A lateral separation existed between the wells of ~18m at the shallowest source receiver position increasing to ~42m at the deepest source/receiver location.

**Stacking**

The AST provides a highly repeatable source, making it ideally suited for stacking to reduce noise levels and improve arrival time detection. In the test well data shown here, noise levels are very low and individual arrivals can be easily identified without stacking. However, this may not represent the typical operating environment.

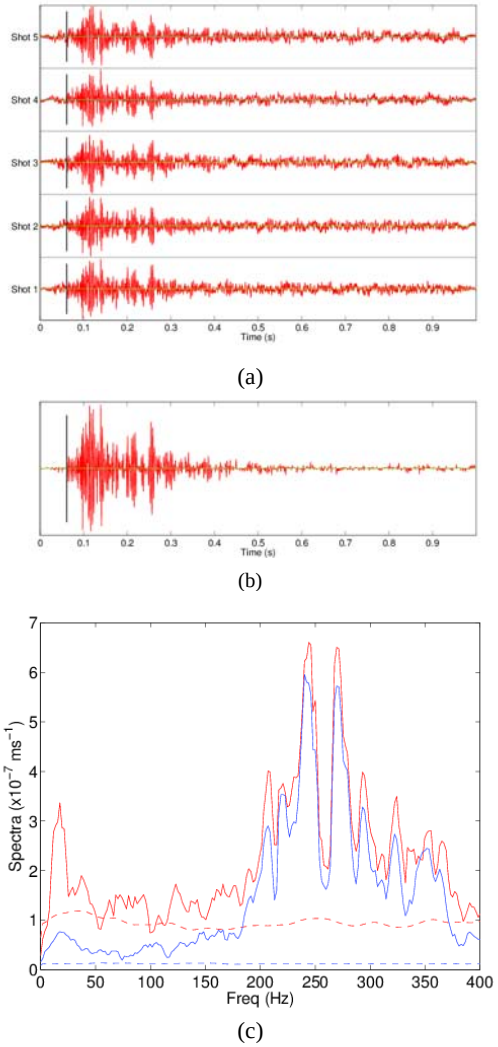


Figure 4: Improvement in signal quality afforded by stacking multiple repeatable source shots. In (a) we show individual shot recordings at a single geophone, with added synthetic noise to reflect the challenges of operation in noisy environments. In (b) we show the composite, stacked trace. The P-wave onset has become much clearer. In (c) we plot spectrograms of the signal (solid lines) and pre-signal noise (dashed lines) for individual shots (red) and stacked traces (blue). Noise levels are substantially reduced by stacking.

In Figure 4 we demonstrate how the repeatable source data can be stacked to substantially improve signal detection. We have added synthetic noise to our raw data to represent more challenging operating conditions (Figure 4a). We then perform a phase-weighted stack (Schimmel and Paulssen, 1997) on 5 individual waveforms, producing the composite

waveform shown in Figure 4b. The improvement in signal detection is clear from examination of the waveforms. In Figure 4c we show the spectra of the unstacked and stacked signals and pre-signal noise. Maximum signal to noise ratios are 14.1 prior to stacking, and 53.7 post stack.

**Construction of velocity models**

In this paper we seek to compare velocity models produced from well log data and from the cross-well survey. We begin by constructing a layered velocity model from the sonic log P-wave velocities, first smoothing the velocity log, before "blocking" it into discrete layers.

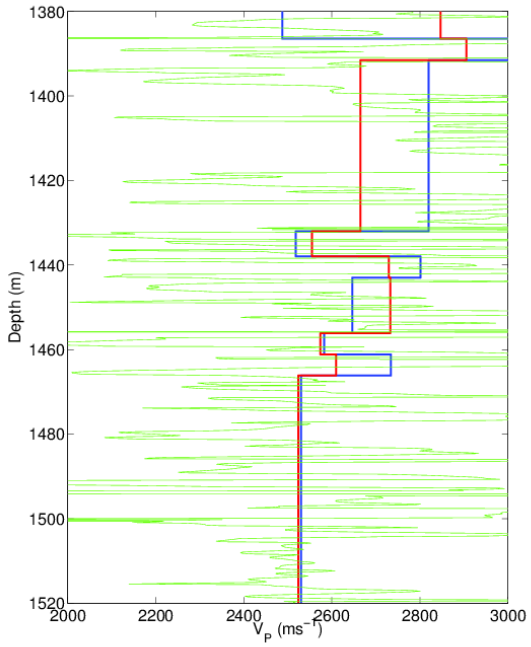


Figure 5: Sonic log velocity data (green), blocked velocity model derived from the log (blue), and velocity model derived from crosswell data (red).

We perform a relatively simple form of cross-well tomography in order to create a 1D, layered model with which to compare with the sonic log-based model, fixing the layer depths to those of the log-based model. We note in passing that the state of the art in cross-well tomography is the full inversion of 2D, and even 3D, velocity heterogeneity (e.g., Ajo-Franklin et al., 2013). We use a neighbourhood algorithm optimization function (Sambridge, 1999) to search for optimum P-wave velocities in each layer to minimize observed and modelled travel times. In Figure 5 we show the P-wave sonic log, the log-derived velocity model, and the velocity model derived from crosswell data. We note broad agreement between log and crosswell-derived models, but also important differences. The average velocity difference between the models is 110ms$^{-1}$ (~4%). In Figure 6 we plot the observed (solid lines) and modelled (dashed lines) arrival times for each shot at each geophone (solid lines). The mean residual is 6x10$^{-4}$s.

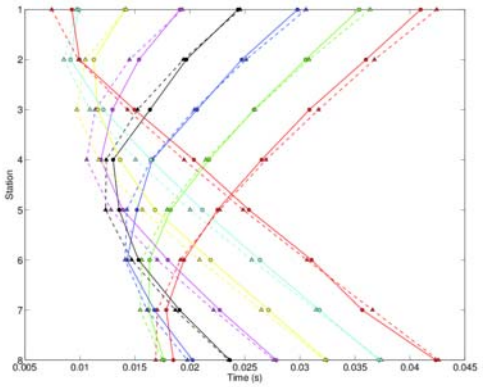


Figure 6: Observed (solid lines) travel times for each shot and receiver, and modeled arrival times for the best-fit velocity model (dashed lines)

**Impact of velocity models on event location**

In order to determine the impact of velocity model errors on event locations, we simulate a population of 200 synthetic events, with spatial positions typical of hydraulic fracture. The events delineate a bi-wing fracture approximately 400m long and 100m high. Injection occurs 150m from the monitoring array of 8 geophones (Figure 7). We compute synthetic "observed" travel times for these events using the crosswell-derived velocity model. The effects of picking errors are incorporated into the synthetic "observed" arrival times, adding errors with a standard deviation of 2ms to P-wave arrivals and 5ms to S-wave arrivals.

Using our synthetically created "observed" arrival times, we compute event locations using both the log-derived and the crosswell-derived velocity models. The difference between the inverted event locations and the known event locations used to create the synthetic datasets will allow us to measure the impact of velocity model choice on event location accuracy. Figure 8 shows location errors in the 'X', 'Y' and 'Z' axes for events located using the crosswell-derived velocity model (Figure 8a), and using the log-derived velocity model (Figure 8b). We note that errors in the 'X' axis (distance along the fracture) are greatest for events at greatest distance from the injection point, while errors in the 'Y' axis and in depth ('Z' axis) are greatest for

events closest to the injection point. More importantly, we note that the differences between log-derived and crosswell-derived velocity models are such that the location errors for events using the log-derived model are on average 50% larger. In particular, we note that errors in depth (green) become particularly pronounced.

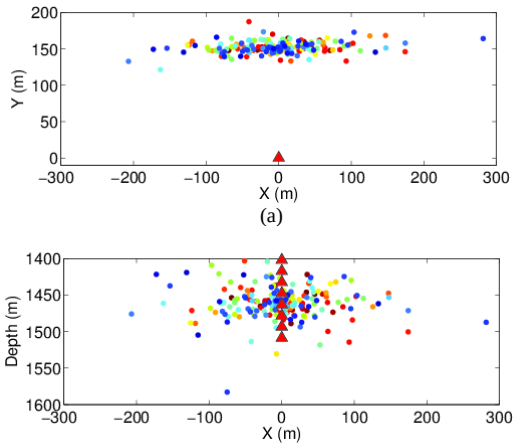


Figure 7: Synthetic event population used to test effects of velocity model on location accuracy, shown in map (a) and cross-section (b). Dots show event locations, triangles show geophone array.

## Conclusions

When comparing the event locations derived from both the cross well tomography velocity model and the sonic data velocity model (Figure 8) we can see a significant contrast in location error. The errors present within locations derived from the sparker crosswell velocities provided a much more constrained distribution, especially on the vertical (Z) axis close to the injection point and on the X- (inline to facture) axis as fracture offset increases.

Going forward, using a downhole source which can deliver quick repeatable signatures which outputs a broadband frequency typical of the monitored microseisms would facilitate and establish a more constrained velocity model prior to injection instead of relying on sonic and single point perforation velocities, which in turn would help minimize microseismic event location error.

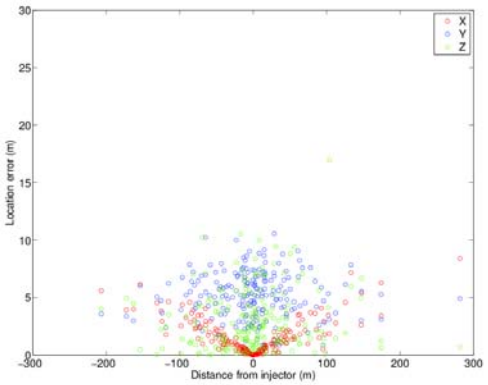


(a) Crosswell-derived velocity model event error distribution

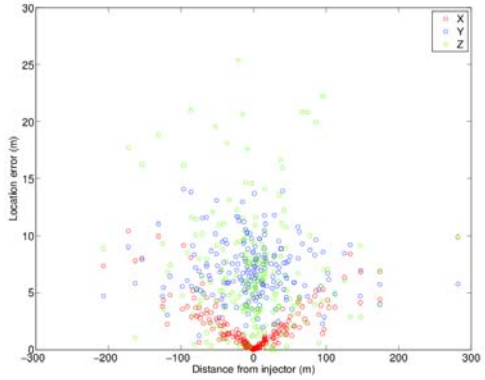


(b) Sonic Log-derived velocity model event error distribution

Figure 8: Location errors in X (red), Y (blue) and Z (green) for events located using the crosswell-derived velocity model (a), and the log-derived velocity model (b).

## Acknowledgments

We would like to thank Li Liu and Halliburton for providing access to the North Belt well site along with relevant sonic log information. The efforts and support from Tom Fryer (ASL) in compiling the data is much appreciated.

## Reducing velocity model uncertainty and improving microseismic event location accuracy: crosswell seismic tomography using a repeatable downhole sparker source.

### References


Ajo-Franklin J.B., Peterson J., Doetsch J., Daley T.M, 2013, High-resolution characterization of a $CO_2$ plume using crosswell seismic tomography: Cranfield, MS, USA: International Journal of Greenhouse Gas Control, **18**, 497-509.

Baltazar-Lopez M., Best S., Brandhorst H.W., Burell Z.B., Heffernan M.E., Rose M.F, 2009, Analysis and simulation of low power plasma blasting for processing lunar material: American Institution of Aeronautics and Astronautics, **4550**, 1-11.

Crosson R.S, 1976, Crustal structure modelling of earthquake data: 1. Simultaneous least squares inversion of hypocentre and velocity parameters: Journal of Geophysical Research, **81**, 3036-3046.

Eisner L., Duncan P., Heigl W.M., Keller W.R, 2009, Uncertainties in passive seismic monitoring: The Leading Edge, **28**, 648-655.

Sambridge M, 1999, Geophysical inversion with a neighbourhood algorithm – I. Searching a parameter space: Geophysical Journal International, **138**, 479-494.

Schimmel M, and Paulssen H, 1997, Noise reduction and detection of weak, coherent signals through phase-weighted stacks: Geophysical Journal International, **130**, 497-505.

Usher P.J., Angus D.A., Verdon J.P, 2013, Influence of a velocity model and source frequency on microseismic waveforms: some implications for microseismic locations: Geophysical Prospecting **61**, 334-345.